PHYSICAL REVIEW C **69**, 064607 (2004)

Induced nucleon polarization and meson-exchange currents in $(e,e'p)$ reactions

F. Kazemi Tabatabaei,[1] J. E. Amaro,[1] and J. A. Caballero[2]
[1]*Departamento de Física Moderna, Universidad de Granada, Granada 18071, Spain*
[2]*Departamento de Física Atómica, Molecular y Nuclear, Universidad de Sevilla, Apdo. 1065, Sevilla 41080, Spain*
(Received 29 January 2004; published 16 June 2004)

Nucleon recoil polarization observables in $(e,e'\vec{p})$ reactions are investigated using a semirelativistic distorted-wave model which includes one- and two-body currents with relativistic corrections. Results for the induced polarization asymmetry are shown for closed-shell nuclei and a comparison with available experimental data for ^{12}c is provided. A careful analysis of meson-exchange currents shows that they may affect significantly the induced polarization for high missing momentum.

DOI: 10.1103/PhysRevC.69.064607 PACS number(s): 25.30.Fj, 24.10.Eq, 24.70.+s, 24.10.Jv

I. INTRODUCTION

Measurements of the polarization of the ejected proton in $(e,e'\vec{p})$ reactions [1] provide valuable information on the nucleus complementary to that extracted from unpolarized experiments [2–5]. In fact, a new set of eight spin-dependent response functions that present different sensitivities to the various ingredients of the reaction mechanism enter in the general analysis [6–8]. A richer source of information on nucleon properties inside the nucleus is thus embedded into the spin-dependent nuclear responses.

In a previous work [9] we have developed a model aiming to provide a systematic investigation of spin-dependent observables in $(\vec{e},e'\vec{p})$ reactions. Relying on the distorted-wave impulse approximation (DWIA), our approach includes, in addition, two-body meson-exchange currents (MEC) and relativistic corrections based on the semirelativistic form of the electromagnetic currents derived in the last years [10–13].

In Ref. [9] the full set of polarized response functions was computed and analyzed for intermediate to high values of the momentum transfer q at the quasielastic peak. Their dependence on the model of final-state interactions (FSI) was studied and the effects of MEC were evaluated. The emphasis was placed on the proton polarization induced by polarized electrons, i.e., on the transferred polarization asymmetries $P'_{l,s}$, which only contribute when the initial electron-beam polarization is measured. These transferred asymmetries survive in the plane-wave impulse approximation (PWIA) limit and may provide ideal tools for studying the electromagnetic nucleon form factors in the nuclear medium [14–17].

The focus of this paper is the analysis of the properties displayed by the polarization observables induced by *unpolarized* electrons, i.e., the induced polarization asymmetry **P** which, contrary to the transferred asymmetries, is zero in PWIA. In fact, since the target nucleus is unpolarized the electron can hit with equal probability nucleons with all spin orientations along their orbits. In the absence of FSI, these nucleons leave the nucleus as plane waves with the same amplitude, hence giving no net-induced polarization. The situation clearly differs when FSI are considered in the description of the process: first, because of the relation between the spin direction and the nucleon location in the orbit, which implies different FSI strengths for different spin orientations due to the central part of the optical potential (mainly the imaginary absorptive term), and second, because of the explicit spin dependence of the spin-orbit interaction in the optical potential.

One of the goals of this work is to evaluate the impact of the two-body MEC over the induced polarization components and hence to analyze the validity of the impulse approximation (IA), i.e., one-body currents only. We are guided by previous studies [9,18], where the role of MEC on asymmetry observables has been found to be in general small for low missing momentum p. This result is in part due to the occurrence of an effective cancellation of MEC effects between the numerators and denominators involved in the polarization ratios. The same applies to FSI effects. However, for higher values of the missing momentum the effective cancellation does not occur and MEC (likewise FSI) effects can be important. Other ingredients not included in the present model, such as correlations [19] and relativistic nuclear dynamics [17,20], have been also shown to sizeably affect the polarization asymmetries at high p.

The structure of the paper is as follows. In Sec. II we shortly present our distorted-wave model. In Sec. III we discuss the results obtained for the induced polarization asymmetry and compare with available data. Finally, the conclusions are drawn in Sec. IV.

II. DWIA MODEL FOR $(e,e'\vec{p})$

We refer to our previous works [9,18], and references therein, for details on the model. Here we just set up some general definitions of interest for the reader and for the discussion that follows. In the $(e,e'p)$ process sketched in Fig. 1, we consider an electron with four-momentum $K_e^\mu=(\varepsilon_e,\mathbf{k}_e)$ that scatters off a nucleus transferring a four-momentum $Q^\mu=(\omega,\mathbf{q})$. The electron-scattering angle is θ_e. A proton with momentum $\mathbf{p}'$ and exit solid angle $\Omega'=(\theta',\phi')$ is detected in coincidence with the outgoing electron. The proton spin polarization along an arbitrary, unitary vector $\vec{s}$, is also measured. We assume that the residual nucleus is left in a discrete state, and neglect the recoil. The cross section for this process can be written in the Born

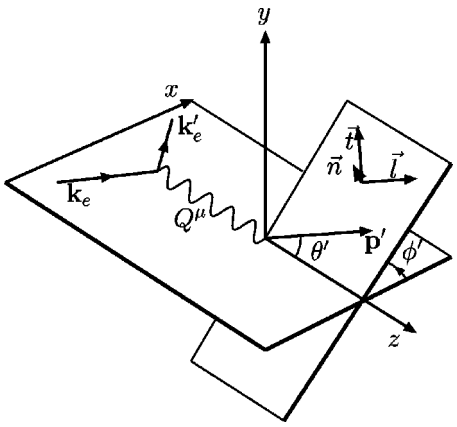

FIG. 1. The coordinate system used in the $(e,e'\vec{p})$ reaction. The x-z coordinates span the scattering plane, with the z axis pointing along the momentum transfer $\mathbf{q}$. The proton polarization is described in the barycentric system (l,t,n), where the ejected nucleon momentum $\mathbf{p}'$ expands the $\vec{l}$ direction, while the $\vec{l}$ and $\vec{t}$ vectors expand the reaction plane. Finally, the normal vector $\vec{n}$ is defined by $\mathbf{q}\times\mathbf{p}'$.

approximation and extreme relativistic limit for the electron as

$$\Sigma \equiv \frac{d\sigma}{d\epsilon'_e d\Omega'_e d\Omega'} = K\sigma_M(v_L R^L + v_T R^T + v_{TL} R^{TL} + v_{TT} R^{TT}), \tag{1}$$

where σ_M is the Mott cross section, K is the kinematic factor $m_N p'/(2\pi\hbar)^3$ (with m_N the nucleon mass), and the v_α coefficients, $\alpha = L,T,TL,TT$, are the usual ones arising from the leptonic tensor [8]. Finally, the exclusive response functions R^α are linear combinations of the hadronic tensor and hence they contain all the pertinent information on the nuclear reaction mechanism.

In the present paper we make use of the semirelativistic distorted-wave model developed in Refs. [9,18], whose basic ingredients are the following: (i) The final proton state is described by a solution of the Schrodinger equation with a nonrelativistic optical potential, but assuming the relativistic energy-momentum relation, thus we effectively solve a Klein-Gordon kind equation. (ii) Semirelativistic (SR) operators are used for the one-body (OB) electromagnetic current and two-body MEC. These have been obtained by expanding the corresponding relativistic operators to first order in the missing momentum over the nucleon mass p/m_N (being $\mathbf{p} = \mathbf{p}' - \mathbf{q}$), while the exact dependence on $(\omega,\mathbf{q})$ is maintained [12,13]. We consider the one-pion exchange diagrams of seagull (S or contact), pion-in-flight (P or pionic), and Δ-isobar kinds.

The induced polarization asymmetry $\mathbf{P}$, which is the focus of this paper, is defined by

$$\Sigma = \frac{1}{2}\Sigma_{unpol}(1 + \mathbf{P}\cdot\vec{s}). \tag{2}$$

The vector $\mathbf{P} = (P_l, P_t, P_n)$ is usually set in the barycentric coordinate system, referred to the reaction plane, as longitudinal $(\vec{l})$, transverse or sideways $(\vec{t})$, and normal $(\vec{n})$ directions defined in Fig. 1.

These induced polarization components can be written in the form

$$P_n = \frac{2}{W_0}(v_L W_n^L + v_T W_n^T + v_{TL}\cos\phi\, W_n^{TL} + v_{TT}\cos 2\phi\, W_n^{TT}), \tag{3}$$

$$P_l = \frac{2}{W_0}(v_{TL}\sin\phi\, W_t^{TL} + v_{TT}\sin 2\phi\, W_l^{TT}), \tag{4}$$

$$P_t = \frac{2}{W_0}(v_{TL}\sin\phi\, W_t^{TL} + v_{TT}\sin 2\phi\, W_t^{TT}), \tag{5}$$

where $\phi = \phi'$ is the azimuthal angle of $\mathbf{p}$, and we have defined the function

$$W_0 \equiv v_L W_0^L + v_T W_0^T + v_{TL}\cos\phi\, W_0^{TL} + v_{TT}\cos 2\phi\, W_0^{TT}, \tag{6}$$

and the unpolarized W_0^α and polarized W_i^α reduced response functions have been introduced. The role of the various ingredients of our model (FSI and MEC) over the separate response functions was analyzed in [9,18]. In the following we show results for the induced polarization components for selected kinematical conditions.

III. RESULTS FOR THE INDUCED POLARIZATION

Since the induced polarization is zero in the absence of FSI, this observable is expected *a priori* to be especially sensitive to details of the optical potential used to describe the final proton state. Results of FSI model dependences are presented in Figs. 2 and 3 for proton knockout from the $p_{1/2}$ and $p_{3/2}$ shells in ^{16}O. Quasiperpendicular kinematics is considered [21,22], with $q = 460$ MeV/c and $\omega = 100$ MeV, corresponding closely to the quasielastic peak. The electron-scattering angle is $\theta_e = 30°$. In Fig. 2 we show results for the normal component P_n for three values of the proton azimuthal angle $\phi = 0$, 90°, and 180° (see definition in Fig. 1). Two optical potentials widely used in the literature to describe these reactions are considered: the Schwandt [23] potential with dashed lines and the Comfort and Karp [24] one with solid lines. Note that the Schwandt potential has been extrapolated here to $A = 16$, since it was fitted for heavier nuclei. These two potentials differ in their spin-orbit dependence. Whereas the Comfort-Karp potential includes a purely real term, Schwandt's has also an imaginary part; moreover, the real part of the Comfort potential is more attractive near the nuclear surface. Concerning the dependence on the real and imaginary parts of the central potential, Schwandt's is more attractive and has less absorption. However, in their gross features the two potentials do not present remarkable discrepancies. This explains why at low missing momentum they provide similar predictions for P_n, starting to differ for higher p values $p > 200$ MeV/c.

The corresponding P_l and P_t polarization components are shown in Fig. 3. Note from Eqs. (4) and (5) that these com-

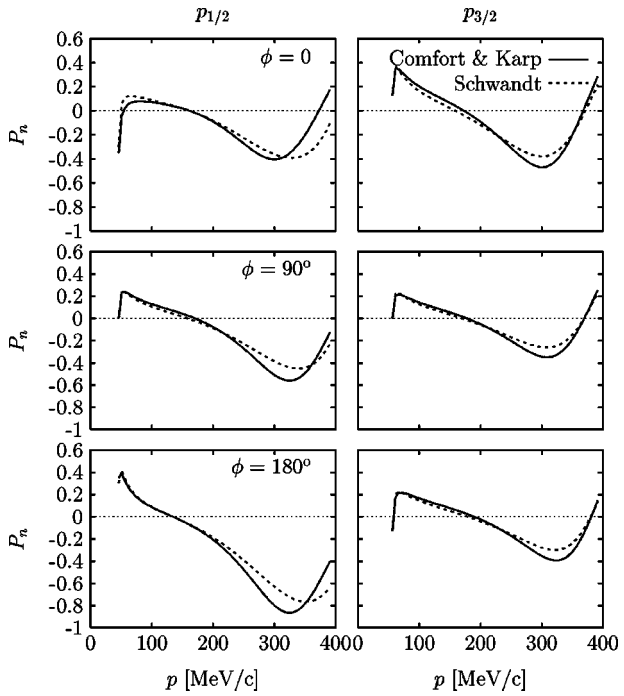

FIG. 2. Proton-induced polarization in the n direction for knockout from the p shells of ^{16}O. The kinematics are q=460 MeV/c, ω=100 MeV, θ_e=30°. The dependence on FSI is analyzed by comparison of two-optical potentials.

ponents are zero for in-plane emission (ϕ=0,180°), hence we only present results for out-of-plane kinematics, ϕ=90°. The biggest differences between both potentials show up in P_l (upper panels) for low and high values of the missing momentum, while P_t (lower panels) exhibits less dependence to details of the potential. The reason why P_l is more sensitive to the details is not clear. However, both polarizations are crucially dependent on the interaction, since they are strictly zero in PWIA. This is clearly illustrated in Fig. 3,

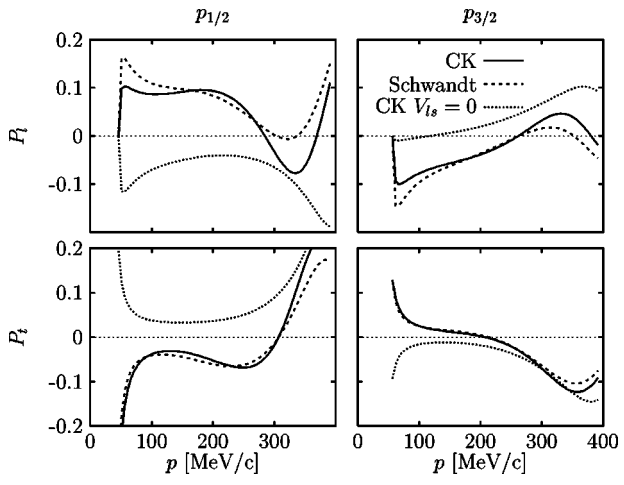

FIG. 3. The same as Fig. 2 for the P_l and P_t polarization components and for ϕ=90°. Note that these observables are zero for in-plane emission (i.e., ϕ=0 or 180°). The dotted lines correspond to the Comfort-Karp potential but neglecting its spin-orbit dependence.

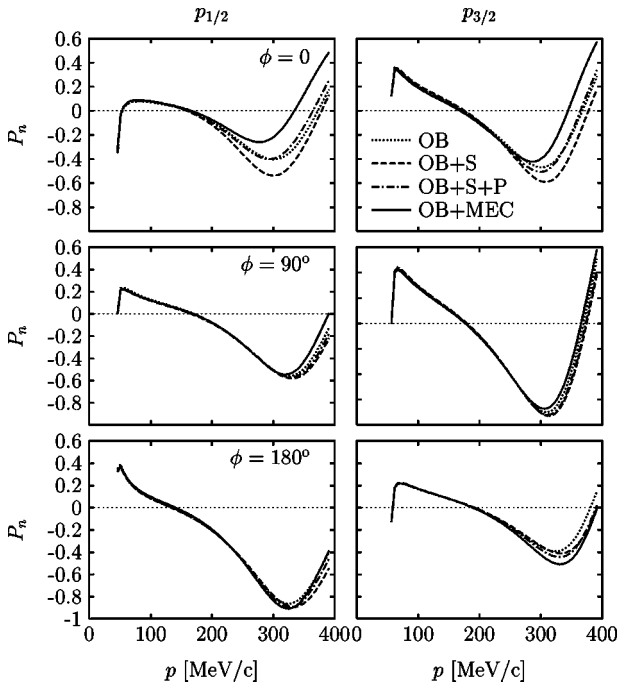

FIG. 4. MEC effects over the proton-induced polarization in the n direction for knockout from the p shells of ^{16}O, q=460 MeV/c, ω=100 MeV, and θ_e=30°.

where we show with dotted lines the results obtained with the Comfort-Karp potential but neglecting its spin-orbit dependence. The drastic change produced in the two polarizations shows that both observables depend equally on the global form of the interaction. However, at the kinematics selected, P_l presents a slightly stronger sensitivity to the "fine" details of the potential.

In the following we analyze the MEC effects, restricting ourselves to the use of the Comfort and Karp potential. Discussion of the results for the Schwandt potential follows similar trends.

In Figs. 4–7 we present the impact of MEC upon the induced polarization components for two values of the momentum transfer. Figure 4 displays the P_n polarization for

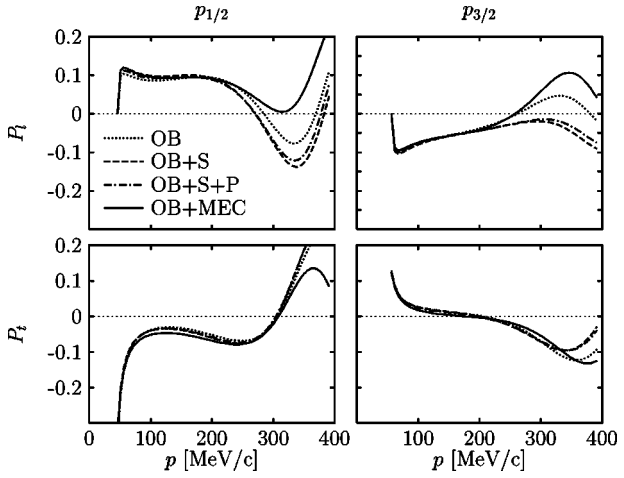

FIG. 5. The same as Fig. 4 for the P_l and P_t polarization components and for ϕ=90°.

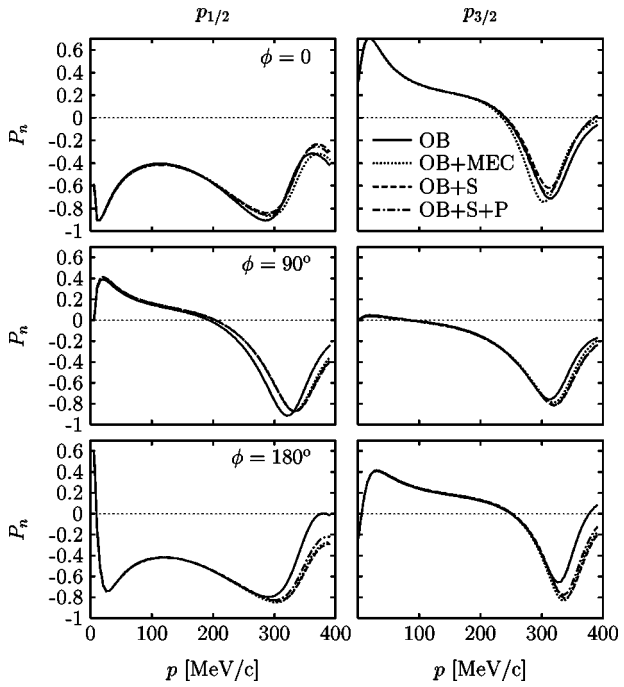

FIG. 6. MEC effects over the proton-induced polarization in the n direction for knockout from the p shells of ^{16}O, $q=1$ GeV/c, $\omega=450$ MeV, and $\theta_e=30°$.

intermediate $q=460$ MeV/c and $\omega=100$ MeV. In addition to the OB calculation (dotted lines), in each panel of Fig. 4 we show three more curves corresponding to the additional contribution of the several MEC: seagull (OB+S), seagull plus pionic (OB+S+P), and total MEC (OB+S+P+Δ). As shown, for low missing momentum MEC contributions are in general negligible, and tend to increase as p goes higher. In particular, for $\phi=0$ (top panels) MEC are shown to significantly modify the results of P_n for $p>200$ MeV/c, this effect being larger for the $p_{1/2}$ shell. For the other ϕ values selected, MEC are smaller for all missing momenta. This outcome, which is specific to the kinematics selected, can be ascribed to a cancellation of the two-body effects in P_n. Note

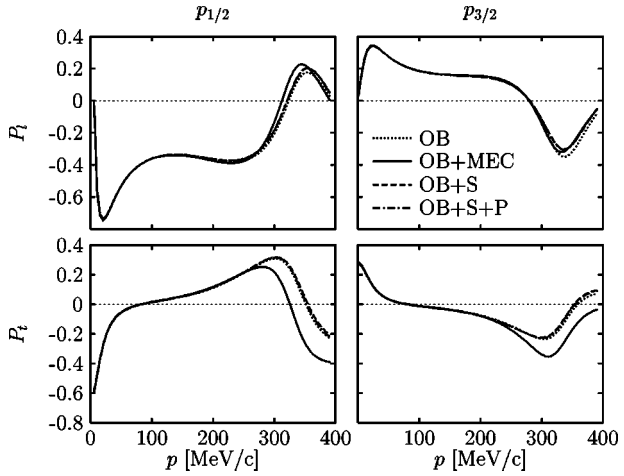

FIG. 7. The same as Fig. 6 for the P_l and P_t polarization components, for $\phi=90°$.

that the contribution of the interference TL response for $\phi=180°$ is just opposite that one occurring at $\phi=0$, while for $\phi=90°$ the TL response does not enter, see Eq. (3).

Larger MEC effects for high missing momentum, $p>200$ MeV/c, are shown in Fig. 5 in the case of the longitudinal and transverse-induced polarizations. Note that P_l (top panels) may even change its global sign when MEC are considered. As in the previous case of P_n, the role of MEC for $p<200$ MeV/c is again negligible. From these results, we may conclude that the description of the induced polarization observables within the IA, i.e., with OB current operators only, is expected to be quite acceptable in this low-p regime.

Concerning the separate role played by the S, P, and Δ currents, the results in Figs. 4 and 5 for high missing momentum, $p>200$ MeV/c, show that the seagull contribution is opposite those provided by the pionic and Δ currents. Quantitatively the importance of the three currents upon P_n for $\phi=0$ is similar. Note also that the P and S contributions tend to cancel in this case. On the contrary, for the transverse-induced polarizations, particularly for P_l, the Δ current is clearly dominant, whereas the pionic current is almost negligible.

Results for higher values of $q=1$ GeV/c and $\omega=450$ MeV are shown in Figs. 6 and 7. This kinematics corresponds to a recent experiment at TJLab [25], where the A_{TL} asymmetry and transfer polarization were measured. The use of the present semirelativistic model for this kinematics is justified by a comparison with the relativistic distorted-wave impulse approximation (RDWIA) calculation of Udias *et al.* [17,26,27]. Although the dynamical relativistic effects that occur in RDWIA have been shown to be important in the high missing momentum region, the results in Figs. 6 and 7 constitute an indication of what kind of effects can be expected from MEC in this region.

As in the previous kinematics, MEC contributions are negligible for low missing momentum, $p\leqslant 200$ MeV/c. This strong MEC suppression is in part due to the behavior of the pion-nucleon form factor at high $|Q^2|$. For higher p values, $p>300$ MeV/c, MEC start to be important, giving a significant contribution for P_n at $\phi=180°$ and P_t at $\phi=90°$. Note the difference with the previous kinematics, where the largest MEC effects were exhibited by P_n at $\phi=0$ and P_l ($\phi=90°$). Particularly noteworthy is also the clear dominance of the Δ current over the P and S terms. These MEC effects are similar to the ones found over the A_{TL} asymmetry for the same kinematics [18].

In Fig. 8 we show results for the normal polarization of proton knockout from the two shells in ^{12}c, including only OB electromagnetic operators. We have chosen three sets of kinematics following closely those of Ref. [1], $q\simeq 760$ MeV/c, and $\omega\simeq 290$ MeV. These values correspond nearly to the quasielastic peak. Since several sets of values have been used in the literature when comparing with the corresponding experimental data, in Fig. 8 we show three curves for three slightly diverse (q,ω) sets. The results for the $p_{3/2}$ shell (upper panel) illustrates that extreme caution is needed before final conclusions can be drawn. In fact, the experimental point at $p\simeq 40$ MeV/c is extremely sensitive to the missing momentum region allowed by the kinematics.

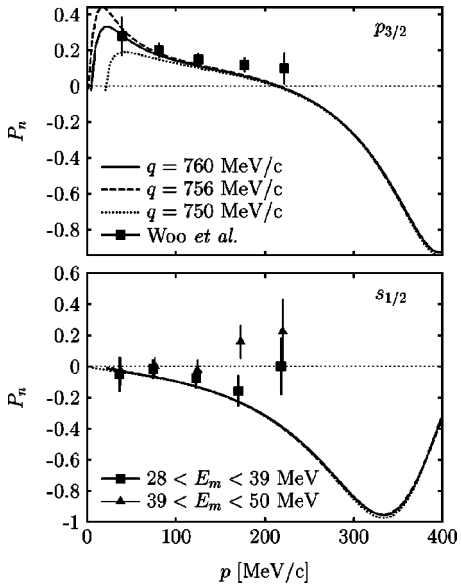

FIG. 8. Normal-induced polarization for ^{12}c computed in DWIA with OB current operators only. The electron energy is $\epsilon_e = 579$ MeV and $\phi = 0°$. Three kinematics close to the quasielastic peak are displayed: $(q,\omega) = (760\ \text{MeV}/c,\ 290\ \text{MeV})$, $(756\ \text{MeV}/c,\ 284\ \text{MeV})$, and $(750\ \text{MeV}/c,\ 294\ \text{MeV})$. The experimental data, corresponding to $|Q^2| = 0.5\ (\text{GeV}/c)^2$, are from Ref. [1].

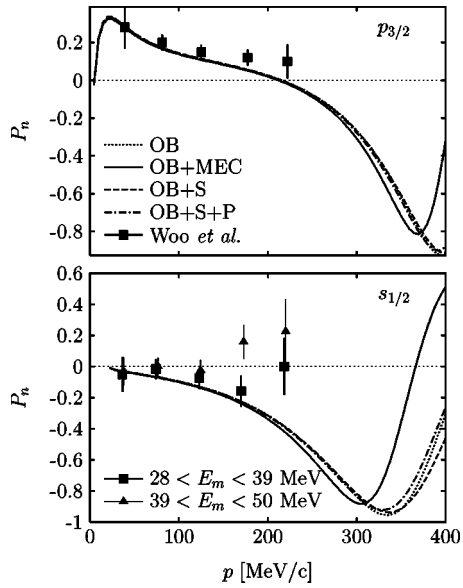

FIG. 9. MEC effects over the normal induced polarization for ^{12}c. The kinematics correspond to Fig. 8 with $(q,\omega) = (760\ \text{MeV}/c,\ 290\ \text{MeV})$. The experimental data are from Ref. [1].

For exact quasielastic conditions, this region begins at $p = 0$, corresponding to the forward emission of a nucleon with momentum $p' = q$. A slight change of (q,ω) can shift the allowed region by more than 25 MeV/c. The large error bars in the first data point are then reminiscent of the large instability of P_n under tiny kinematical variations. The remaining data points located in the region of larger missing momentum, and the case of the $s_{1/2}$ shell, where a great stability exists, are of more physical interest for the analysis of two-body currents.

Regarding MEC effects upon P_n in ^{12}c, we show in Fig. 9 the comparison between our calculations including the OB and the several pieces of the two-body current. In the region of low missing momentum, $p < 200$ MeV/c, where experimental data are located, MEC contributions are negligible for both shells. As in the case of ^{16}O, here MEC lead to significant effects, particularly due to Δ which gives the main contribution, in the high missing momentum region $p > 300$ MeV/c. Results in Fig. 9 also show that the SR distorted-wave model calculations agree nicely with data. Moreover, the discrepancy with the results obtained within the RDWIA framework [20,28], which is better suited to describe these high (q,ω) data, is small in the low missing momentum region, and begin to be important for $p \sim 200$ MeV/c. For larger missing momenta, $p > 300$ MeV/c, dynamical relativity, not included in our calculations, plays an important role and differences between RDWIA and SR-DWIA calculations increase. Note however, that MEC make also a very significant effect in this high-p region.

To finish we compare our results with the previous calculations of MEC effects over the induced polarization asymmetries, namely with the models developed by the Gent [15] and Pavia [29] groups. In the Gent calculation [15], MEC contributions upon P_n for ^{12}c were also found to be very small for low missing momentum, while they increase importantly, particularly due to Δ, for high p. Discrepancies with our results emerge because of the different models used to describe FSI; the Gent group makes use of a real potential without absorption. In the case of the Pavia calculation [29], the induced polarization was evaluated for low missing momentum, $p < 200$ MeV/c, and FSI were computed by means of complex phenomenological optical potentials. Their P_n results for ^{16}O with the Giannini and Rico optical potential [30], and a kinematics close to the one of Fig. 4, are similar to ours. MEC effects were found to be small in general, specially for the $p_{3/2}$ shell, while for $p_{1/2}$ some visible differences, strongly dependent on the specific optical potential used, show up even within this low-p regime. This outcome contrasts our calculations, which do not show any specific difference between both shells.

IV. CONCLUSIONS

In this work we have analyzed the induced polarization asymmetry of knocked-out protons in exclusive $(e,e'p)$ reactions to discrete residual nucleus states. We have used a semirelativistic distorted-wave model including relativistic corrections to the one- and two-body currents, as well as relativistic kinematics. We have applied the model to proton knockout from the outer shells of ^{16}O and have compared it with the experimental data available for ^{12}c.

Regarding FSI, the P_n polarization is little dependent on the details of the optical potential for low missing momentum, while its dependence increases for high p. The longitudinal P_l polarization is more sensitive to details of the poten-

tial both for low and high values of p, while the sideways P_t polarization only shows tiny FSI uncertainties for $p > 300$ MeV/c.

Concerning MEC, they are negligible for low $p < 200$ MeV/c, but they can importantly change the induced polarization components for high p. In this regime the largest MEC contributions are found for intermediate values of the momentum transfer. The effects upon P_n are in accordance with the Gent calculation, even if differences emerge due to the different FSI models used. The comparison with the older Pavia calculation, which gives rise to some peculiar differences between the two p shells in ^{16}O, is more troublesome.

The present calculation justifies the validity of the impulse approximation for $p < 200$ MeV/c, while it emphasizes the fact that, besides dynamical relativity, other effects beyond the IA as MEC are also expected to contribute sizeably for high missing momentum. New experimental data for these observables in this regime would be welcomed to explore this physics.

ACKNOWLEDGMENTS

This work was partially supported by funds provided by DGI (Spain) and FEDER, under Contract Nos. BFM2002-03218, BFM2002-03315, and FPA2002-04181-C04-04, and by the Junta de Andalucía.

[1] R.J. Woo *et al.*, Phys. Rev. Lett. **80**, 456 (1998).
[2] S. Frullani and J. Mougey, Adv. Nucl. Phys. **14**, 1 (1984).
[3] S. Boffi, C. Giusti, and F.D. Pacati, Phys. Rep. **226**, 1 (1993).
[4] J.J. Kelly, Adv. Nucl. Phys. **23**, 75 (1996).
[5] S. Boffi, C. Giusti, F.D. Pacati, and M. Radici, *Electromagnetic Response of Atomic Nuclei* (Oxford University Press, Oxford, 1996).
[6] A. Picklesimer and J.W. Van Orden, Phys. Rev. C **35**, 266 (1987).
[7] A. Picklesimer and J.W. Van Orden, Phys. Rev. C **40**, 290 (1989).
[8] A.S. Raskin and T.W. Donnelly, Ann. Phys. (N.Y.) **191**, 78 (1989).
[9] F. Kazemi Tabatabaei, J.E. Amaro, and J.A. Caballero, Phys. Rev. C **68**, 034611 (2003).
[10] J.E. Amaro, J.A. Caballero, T.W. Donnelly, E. Moya de Guerra, A.M. Lallena, and J.M. Udías, Nucl. Phys. **A602**, 263 (1996).
[11] J.E. Amaro, M.B. Barbaro, J.A. Caballero, T.W. Donnelly, and A. Molinari, Nucl. Phys. **A643**, 349 (1998).
[12] J.E. Amaro, M.B. Barbaro, J.A. Caballero, T.W. Donnelly, and A. Molinari, Phys. Rep. **368**, 317 (2002).
[13] J.E. Amaro, M.B. Barbaro, J.A. Caballero, T.W. Donnelly, and A. Molinari, Nucl. Phys. **A723**, 181 (2003).
[14] S. Malov *et al.*, Phys. Rev. C **62**, 057302 (2000).
[15] J. Ryckebusch, D. Debruyne, W. Van Nespen, and S. Janssen, Phys. Rev. C **60**, 034604 (1999).
[16] J.J. Kelly, Phys. Rev. C **59**, 3256 (1999); **60**, 044609 (1999).
[17] M.C. Martínez, J.R. Vignote, J.A. Caballero, T.W. Donnelly, E. Moya de Guerra, and J.M. Udías, Phys. Rev. C **69**, 034604 (2004).
[18] J.E. Amaro, M.B. Barbaro, J.A. Caballero, and F. Kazemi Tabatabaei, Phys. Rev. C **68**, 014604 (2003).
[19] M. Mazziotta, J.E. Amaro, and F. Arias de Saavedra, Phys. Rev. C **65**, 034602 (2002).
[20] J.M. Udias and J.R. Vignote, Phys. Rev. C **62**, 034302 (2000).
[21] L. Chinitz *et al.*, Phys. Rev. Lett. **67**, 568 (1991).
[22] G.M. Spaltro, H.P. Blok, E. Jans, L. Lapikas, M. van der Schaar, G. van der Steenhoven, and P.K.A. de Witt Huberts, Phys. Rev. C **48**, 2385 (1993).
[23] P. Schwandt *et al.*, Phys. Rev. C **26**, 55 (1982).
[24] J.R. Comfort and B.C. Karp, Phys. Rev. C **21**, 2162 (1980).
[25] J. Gao and the Jefferson Lab Hall A Collaboration, Phys. Rev. Lett. **84**, 3265 (2000).
[26] J.M. Udías, J.A. Caballero, E.Moya de Guerra, J.E. Amaro, and T.W. Donnelly, Phys. Rev. Lett. **83**, 5451 (1999).
[27] J.M. Udías, J.A. Caballero, E. Moya de Guerra, J.R. Vignote, and A. Escuderos, Phys. Rev. C **64**, 024614 (2001).
[28] J.I. Johanson and H.S. Sherif, Phys. Rev. C **59**, 3481 (1999).
[29] S. Boffi, C. Giusti, F.D. Pacati, and M. Radici, Nucl. Phys. **A518**, 639 (1990).
[30] M.M. Giannini and G. Ricco, Ann. Phys. (N.Y.) **102**, 458 (1976).